Hindawi
Advances in Materials Science and Engineering
Volume 2021, Article ID 7570359, 16 pages
https://doi.org/10.1155/2021/7570359

Research Article

Deformation Characteristics of the Surrounding Rock of a Six-Lane Multiarch Tunnel under Different Excavation Conditions

Lina Luo,[1] **Gang Lei**,[2,3] **and Haibo Hu**[2]

[1]*Guangzhou Railway Polytechnic, Guangzhou 510430, China*
[2]*Research Center of Coastal and Urban Geotechnical Engineering, Zhejiang University, Hangzhou 310058, China*
[3]*Beijing Urban Construction Design & Development Group Company Limited, Beijing 100037, China*

Correspondence should be addressed to Lina Luo; luolina@gtxy.edu.cn and Haibo Hu; huhaibo@zju.edu.cn

Received 11 October 2021; Accepted 1 November 2021; Published 24 November 2021

Academic Editor: bingxiang yuan

Highway tunnel plays an increasingly prominent role in the development of high-grade highway traffic in mountainous countries or regions. Therefore, it is necessary to explore the deformation characteristics of the surrounding rock of a six-lane multiarch tunnel under different excavation conditions. Using the three-dimensional indoor model test and finite element analysis, this paper studies the dynamic mechanical behavior of a six-lane construction, reveals the whole process of the surrounding rock deformation process of class II surrounding rock under different excavation conditions, and puts forward the best construction and excavation method. The results show that the maximum displacement rate of excavation scheme III is the largest, and the maximum displacement rate of excavation scheme I is basically the same as that of excavation scheme II. Therefore, in terms of controlling the displacement rate of the surrounding rock, the effect of excavation scheme I is basically the same as that of excavation scheme II, while that of excavation scheme III is poor. In terms of construction technology, scheme II is simpler than scheme I and can ensure the integrity of the secondary lining. Therefore, in class II surrounding rock of the supporting project, it is recommended to adopt scheme II for construction.

1. Introduction

In recent years, civil engineering has developed rapidly [1–6]. As an important structural form of civil engineering, highway tunnel plays an increasingly prominent role in the development of high-grade highway traffic in mountainous countries or regions [7–9]. The tunnel scheme can shorten the mileage, improve the line shape, and protect the environment. As one of the tunnel types, multiarch tunnel can not only meet the requirements of separating the up-traffic and down-traffic, but also has greater advantages than separated tunnel in the plane line type, portal location selection, and land occupation. Therefore, this kind of tunnel is widely used in expressways and first-class highways [10, 11]. At the same time, with the development of the economy and an increase in the traffic volume, the two-way four-lane multiarch tunnel cannot meet the traffic volume requirements in some areas and trunk lines, and hence, a two-way six-lane multiarch tunnel has been built.

Because of the diversity and complexity of the geological conditions of the tunnel surrounding rock and the uncertainty of the stress of the tunnel support structure, the design and construction of the tunnel engineering structure are still in a semitheoretical and semiempirical state, and the theoretical calculation is mainly used as qualitative analysis [12–16]. The large excavation span of a multiarch tunnel, coupled with many factors, such as the interaction caused by excavation, multiple disturbances of the surrounding rock, and asynchronous construction between the support and lining during the construction of the two main tunnels, makes its stress conditions extremely complex. Therefore, for a multiarch tunnel, on-site monitoring, measurement, and back analysis are important means for many scholars to timely grasp the dynamic changes of surrounding rock and the stress of supporting structure, especially under complex geological conditions. Miura et al. comprehensively measured and analyzed the new Tomei Meishin on the Tokyo-Kobe expressway and compared it with the four-lane tunnel

[17]. Wu et al. studied the blasting vibration control of a multiarch tunnel by a field test [18]. Liu et al. introduced in detail the on-site monitoring results of deformation during the construction of a multiarch tunnel of the Beijing-Zhuhai expressway using the three-pilot tunnel method, and they put forward measures to restrain the excessive deformation of the surrounding rock [19]. Relying on the Hejiadaling compound curved middle wall multiarch tunnel on Yuening Avenue, Yang et al. analyzed the development and distribution law of the wall body stress and wall bottom pressure of the composite curved middle wall by on-site monitoring and measurement data [20].

With the rapid development of computer and information technology, numerical simulation technology has been widely used in the research of the multiarch tunnel [21, 22]. Many scholars have used the numerical simulation method to study the multiarch tunnel. Yoshimura et al. studied the deformation law of the surrounding rock during the whole construction process of the Xinaofa multiarch tunnel and verified the correctness of the finite element simulation calculation using the comparative analysis of the predicted and measured values [23]. Chikora et al. simulated and analyzed the tunnel excavation process using the stiffness reduction method and stress reduction method [24]. Lee and Rowe conducted a sensitivity study of the finite element input parameters and simulation results [25]. Li et al. studied the seepage of the subsea tunnel through the model test and numerical simulation [26].

As for the model test research of the multiarch tunnel, Li et al. carried out the proportional physical model test and numerical simulation for a shallow buried multiarch tunnel [10]. Liu et al. studied the acceleration response of the shallow buried biased multiarch tunnel by combining the shaking table test and numerical simulation [27]. Using the method of numerical simulation and model test, Min et al. studied the real three-dimensional response of asymmetric multiarch tunnel structure caused by a cavity [28]. At present, there is little research on the model test for a two-way six-lane highway multiarch tunnel under different excavation conditions.

As an underground project, the rock mass of tunnel engineering has experienced a long-term geological tectonic movement and formed a certain structure in a certain geological environment. This structure will inevitably show a changeable material response range. Its engineering mechanical behavior and deformation and failure mechanism are random and fuzzy, i.e., uncertain, in both subjective and objective aspects. Because of the limitation, incompleteness, and insufficiency of obtaining information and data, it is uncertain. In view of these mechanical characteristics of geotechnical engineering such as tunnels, although advanced mathematics and mechanics are still the necessary and indispensable means to solve engineering problems, the use of the similarity theory and model test is conducive to highlight the main contradictions in the complex test process and to grasp and discover the essential characteristics and internal relations of the phenomena. Therefore, the model test has increasingly become an important means for many scholars at home and abroad to carry out geotechnical engineering research.

This paper will study the dynamic mechanical behavior of six-lane construction using the three-dimensional indoor model test and finite element analysis, and it will reveal the whole process of surrounding rock deformation of class II surrounding rock under different excavation conditions. The deformation characteristics of the surrounding rock of a six-lane multiarch tunnel under different excavation conditions are analyzed, and the best construction and excavation method is put forward.

2. Materials and Methods

2.1. Test Equipment. Using the similar model test method to study the construction mechanical form of a mountain highway tunnel, take a square plane twice the tunnel span and a research unit including the tunnel as the research object. There are two common methods to simulate tunnel excavation. The first is the hollow body loading scheme. When the model is formed, the cavity is reserved to simulate the tunnel, and the external loading simulates the external boundary conditions and initial stress state. Using this model, the static mechanical form of the structure and surrounding rock can be simulated. Using this model to study the mechanical problems of tunnel construction is obviously unreasonable, and its physical process is different from reality. The second model is the test body model. The drill bit excavation simulates tunnel excavation, which solves the problem of excavation distortion. However, it cannot test the displacement of the model tunnel peripheral wall. It is difficult to simulate the tunnel support lining, and it cannot simulate the whole process of tunnel construction.

Researchers hope to design a set of test system, which can not only simulate the construction of tunnel or underground engineering in an all-round way, but also study the mechanical form of tunnel construction through testing. Therefore, based on the above two models, a third model is developed, i.e., the highway tunnel similar model test system with loading first and then tunneling. The specific idea is as follows: the inner wall loading system located in the middle of a similar model is used to simulate the actual tunnel, and the boundary line between the inner wall and the model is just the inner contour of the actual tunnel. The cross section can be in the form of a single center circle or three-center circle to control the two dimensions of the clear width and clear height of the tunnel and ensure that the difference of the inner space area of the tunnel is less than 5%.

The system adopts the graded loading method of "loading first and then excavation," which makes the model excavation method in the laboratory completely consistent with the on-site construction process of the tunnel to solve the problem of similar construction state of the highway tunnel. The system is shown in Figure 1. The size of the model specimen is $240\,\text{cm} \times 160\,\text{cm} \times 160\,\text{cm}$, and the size of the peripheral frame reaction system is $500\,\text{cm} \times 500\,\text{cm} \times 480\,\text{cm}$.

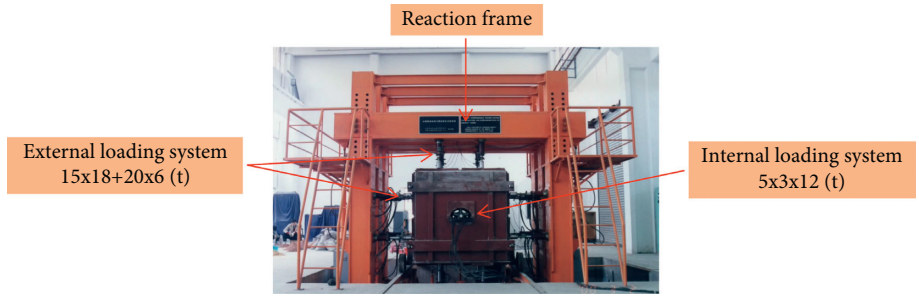

Figure 1: Comprehensive experimental system of highway tunnel and surrounding rock.

The system consists of four subsystems, namely, the external loading subsystem, internal loading subsystem, data acquisition and analysis subsystem, and similarity model-making subsystem.

2.2. Materials. The designed clear span of the single tunnel simulated in this experiment is 15.28 m, the clear height is 8.12 m, the clear span of the double tunnel is 32.15 m, and the geometric similarity ratio of the model is 45. The surrounding rock is a weakly weathered sandstone, belonging to class II surrounding rock. Density is obtained by dividing mass by volume. Uniaxial compressive strength, Poisson's ratio, and elastic modulus are obtained according to the improved Instron electrohydraulic servo fatigue testing machine (Figure 2). Cohesion and internal friction angle are obtained from shear test. See Table 1 for specific material parameters.

2.3. Test Procedure. The main process of this test is material preparation, model making, model forming, and model test. The main test process is shown in Figure 3.

This experiment will study the deformation characteristics of the surrounding rock of a six-lane multiarch tunnel under different excavation conditions, and hence, three different excavation conditions are designed. Excavation scheme I adopts the secondary lining section pouring three heading method, and the simulation sequence of excavation is shown in Table 2. Excavation scheme II adopts the two lining integral pouring three heading method, and the simulation sequence of excavation is shown in Table 3. Excavation scheme III adopts the bench method of middle pilot tunnel, and the simulation sequence of excavation is shown in Table 4.

3. Experimental Results Analysis

In this experiment, the three groups of model tests were carried out, and each group of model tests had a total of 12 sections. Before analyzing the test data, the function fitting of the test data was carried out. In order to facilitate the analysis, the typical section L3 was used for fitting analysis.

The surrounding rock of the six-lane multiarch tunnel is greatly disturbed by mutual construction, and the shape of displacement duration curve is complex because of the influence of this construction disturbance. While carrying out the fitting analysis, it is difficult to use a curve for accurate fitting. After carrying out the fitting analysis using the polynomial and exponential functions, it is found that when using common fitting functions, such as the polynomial and exponential functions, the R square value is often small, the σ^2 value is large, and the fitting degree is very poor. In particular, when using a high-order polynomial fitting, there will be multiple extreme points that have a large error with the actual curve shape. In this study, the Hill function is used for fitting, and its fitting degree is relatively the best. The expression of Hill function is as follows:

$$y = A\frac{x^n}{B^n + x^n}, \tag{1}$$

where A, B, and n are regression coefficients.

The displacement duration curve of typical section L3 under the conditions of three excavation schemes is shown in Figures 4–6.

The fitting function of a typical section displacement curve of each excavation scheme is shown in Table 5.

When excavation schemes I, II, and III are adopted, the corresponding maximum displacements of the surrounding rock are 0.23 mm, 0.27 mm, and 0.29 mm, respectively (as shown in Table 6). During the model test, the effect of the initial support and secondary lining is not simulated, and the final displacement values of each measuring point corresponding to each excavation scheme are relatively close. The maximum displacement values of each excavation scheme are not very different. However, from the numerical analysis of the displacement of each measuring point, it can be seen that, in terms of controlling the surrounding rock stability, excavation scheme I should be better than excavation schemes II and III. Excavation scheme II is better than excavation scheme III.

After comparing and analyzing the curve slope (displacement rate) of each displacement duration curve, it can be found that, under all excavation schemes, the curve slope of each measuring point is the largest at the current step of excavation, i.e., the displacement rate is the largest at the current step of excavation. At the same time, through the analysis of the maximum displacement rate of each excavation scheme, it can be seen that the maximum displacement rate of excavation scheme III is the largest, and the maximum displacement rate of excavation scheme I is basically the same as that of excavation scheme II. Therefore, in terms of controlling the displacement rate of the

Figure 2: The improved Instron electrohydraulic servo fatigue testing machine.

Table 1: Main physical and mechanical parameters of surrounding rock.

Density (g/cm^3)	Uniaxial compressive strength (MPa)	Poisson's ratio	Elastic modulus (GPa)	Cohesion c (kPa)	Internal friction angle φ (°)
1.9	21.3	0.4	1.5	100	37

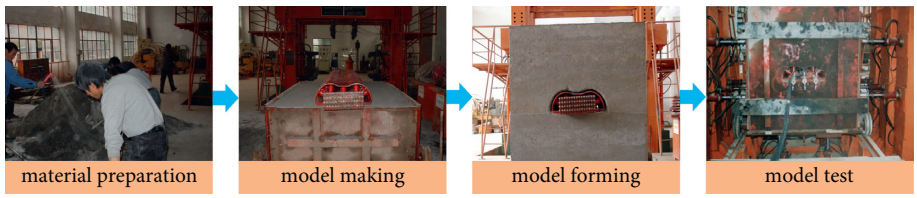

Figure 3: Main test procedure.

Table 2: Excavation sequence of excavation scheme I.

Section number	L1	L2	L3	L4	L5	L6	L7	L8	L9	L10	L11	L12
Left hole	L1-1	L2-1	L3-1	L4-1	L5-1	L6-1	L7-1	L8-1	L9-1	L10-1	L11-1	L12-1
	14	15	16	17	18	19	20	21	22	23	24	25
	L1-2	L2-2	L3-2	L4-2	L5-2	L6-2	L7-2	L8-2	L9-2	L10-2	L11-2	L12-2
	30	31	32	33	34	35	36	37	38	39	40	41
Middle wall	L1-3	L2-3	L3-3	L4-3	L5-3	L6-3	L7-3	L8-3	L9-3	L10-3	L11-3	L12-3
	1	2	3	4	5	6	7	8	9	10	11	12
Right hole	L1-4	L2-4	L3-4	L4-4	L5-4	L6-4	L7-4	L8-4	L9-4	L10-4	L11-4	L12-4
	27	28	29	30	31	32	33	34	35	36	37	38
	L1-5	L2-5	L3-5	L4-5	L5-5	L6-5	L7-5	L8-5	L9-5	L10-5	L11-5	L12-5
	14	15	16	17	18	19	20	21	22	23	24	25

Note. Step 13 is the middle wall support, step 26 is the sidewall support, L* – *represents the template number, and number represents the excavation step.

surrounding rock, the effect of excavation scheme I is the same as that of excavation scheme II, while that of excavation scheme III is poor.

The overall shape of the displacement duration curve is the same as that of the general tunnel, i.e., it is still in the S-shape, and the displacement increases step by step with the excavation step. However, because of the construction of the middle wall, the displacement curve of measuring point 3 (the measuring point on the top of the middle wall) is different from the S-shape, i.e., the displacement does not increase after the construction of the middle wall.

During the construction of the advanced main tunnel, the displacement of the measuring points within a certain range of the later main tunnel changes. Similarly, during the construction of the later main tunnel, the displacement of the surrounding rock within a certain range of the advanced

Table 3: Excavation sequence of excavation scheme II.

Section number	L1	L2	L3	L4	L5	L6	L7	L8	L9	L10	L11	L12
Left hole	L1-1	L2-1	L3-1	L4-1	L5-1	L6-1	L7-1	L8-1	L9-1	L10-1	L11-1	L12-1
	14	15	16	17	18	19	20	21	22	23	24	25
	L1-2	L2-2	L3-2	L4-2	L5-2	L6-2	L7-2	L8-2	L9-2	L10-2	L11-2	L12-2
	29	30	31	32	33	34	35	36	37	38	39	40
Middle wall	L1-3	L2-3	L3-3	L4-3	L5-3	L6-3	L7-3	L8-3	L9-3	L10-3	L11-3	L12-3
	1	2	3	4	5	6	7	8	9	10	11	12
	L1-4	L2-4	L3-4	L4-4	L5-4	L6-4	L7-4	L8-4	L9-4	L10-4	L11-4	L12-4
Right hole	26	27	28	29	30	31	32	33	34	35	36	37
	L1-5	L2-5	L3-5	L4-5	L5-5	L6-5	L7-5	L8-5	L9-5	L10-5	L11-5	L12-5
	14	15	16	17	18	19	20	21	22	23	24	25

Note. Step 13 is the middle wall support, L* – *represents the template number, and number represents the excavation step.

Table 4: Excavation sequence of excavation scheme III.

Section number	L1	L2	L3	L4	L5	L6	L7	L8	L9	L10	L11	L12
Left hole	L1-1	L2-1	L3-1	L4-1	L5-1	L6-1	L7-1	L8-1	L9-1	L10-1	L11-1	L12-1
	23	24	25	26	27	28	29	30	31	32	33	34
	L1-2	L2-2	L3-2	L4-2	L5-2	L6-2	L7-2	L8-2	L9-2	L10-2	L11-2	L12-2
	20	21	22	23	24	25	26	27	28	29	30	31
Middle wall	L1-3	L2-3	L3-3	L4-3	L5-3	L6-3	L7-3	L8-3	L9-3	L10-3	L11-3	L12-3
	1	2	3	4	5	6	7	8	9	10	11	12
	L1-4	L2-4	L3-4	L4-4	L5-4	L6-4	L7-4	L8-4	L9-4	L10-4	L11-4	L12-4
Right hole	14	15	16	17	18	19	20	21	22	23	24	25
	L1-5	L2-5	L3-5	L4-5	L5-5	L6-5	L7-5	L8-5	L9-5	L10-5	L11-5	L12-5
	17	18	19	20	21	22	23	24	25	26	27	28

Note. Step 13 is the middle wall support, L* – *represents the template number, and number represents the excavation step.

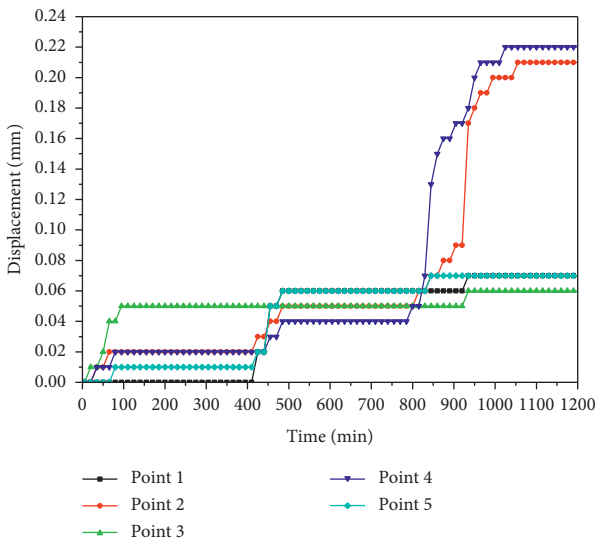

Figure 4: Displacement duration curve of L3 section in excavation scheme I.

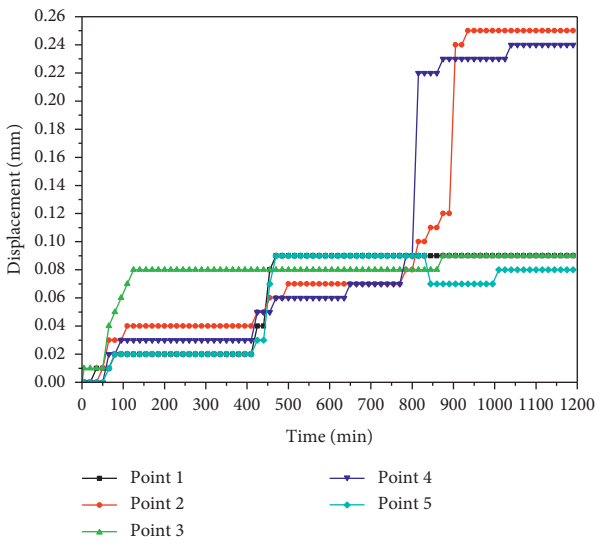

Figure 5: Displacement duration curve of L3 section in excavation scheme II.

main tunnel also changes. It shows that, during the construction of the two main tunnels, the surrounding rock disturbance is obvious, especially during the excavation of the advanced main tunnel.

The displacement of most measuring points is the largest when excavating the current section, and its displacement is generally more than 40% of the final displacement of measuring points. This proportion is smaller than that of the separated tunnel with the same width, mainly because the surrounding rock of the two main tunnels will be disturbed each other during construction, resulting in the continuous displacement of the surrounding rock of the other tunnel.

As the construction of the advanced main tunnel has a great disturbance to the surrounding rock of the later main

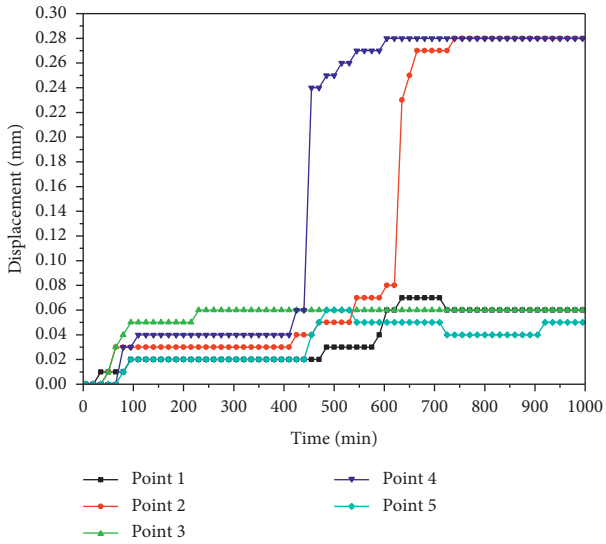

Figure 6: Displacement duration curve of L3 section in excavation scheme III.

tunnel, most of the displacement of the surrounding rock vault of the later main tunnel is greater than that of the corresponding measuring point of the advanced main tunnel.

When the arch crown is excavated, the displacement of measuring point 1 or measuring point 5 tends to decrease. It shows that, in a large-section multiarch tunnel, when the lateral pressure coefficient of the surrounding rock is large, the arch excavation will cause the outward expansion of the surrounding rock at the arch waist. During the construction of a multiarch tunnel, special attention should be paid to this expansion phenomenon to avoid accidents.

From the comparison of the displacements of different measuring points on the same section, it can be seen that the displacement of the arch crown is much greater than that of the other measuring points, i.e., the settlement of the arch crown is much greater than the horizontal convergence, especially the displacement of the sidewall (measuring points 1 and 5) is small, and some displacements expand outward. It shows that, for a large cross-section multiarch tunnel, after the surrounding rock excavation, the soil in the arch deforms into the tunnel under the action of self-weight stress field, resulting in the compression of soil on both sides. Therefore, for a six-lane multiarch tunnel, the vault subsidence should be the key factor of the surrounding rock stability criterion.

The influence range of four-lane separated tunnel excavation is generally about 1 time of the tunnel span in front of the working face to 2~3 times of the tunnel span behind the working face. For the six-lane multiarch tunnel, it can be seen from the shape and trend of the displacement duration curve that the influence range of the left and right tunnel construction on the surrounding rock is larger than that of the separated tunnel; especially, the influence range of the excavation of the rear main tunnel on the surrounding rock displacement is more than 3 times the tunnel span before and after the excavation surface.

Based on the above analysis, it can be seen that, in terms of controlling the stability of the surrounding rock, the effect of the secondary lining segmental pouring three heading method (scheme I) is roughly the same as that of secondary lining integral pouring three heading method (scheme II), which can ensure the basic stability of the surrounding rock. The step method of middle pilot tunnel (scheme III) is poor. In terms of construction technology, the integral pouring three heading method of secondary lining (scheme II) is simpler than the segmental pouring three heading method of secondary lining (scheme I), and it can ensure the integrity of secondary lining. Therefore, in class II surrounding rock of the supporting project, it is recommended to use the secondary lining integral pouring three heading method (scheme II) for construction.

4. Finite Element Analysis

4.1. Program Introduction. 2D-σ program is a commercial software package successfully developed by Softbrain Co. Ltd. and put to the market. It has the following outstanding characteristics: it realizes the organic combination of rapid modeling of finite element method, automatic mesh generation and optimization adjustment, visualization of analysis results, and screen operation. It can easily reproduce the stage or divisional construction process of the site and automatically complete the optimization treatment. The embedded file processing system can easily print charts, reports, and papers.

4.2. Construction Scheme and Model Parameters. The three construction schemes and material parameters are consistent with the model test. The design clear span of a single tunnel is 15.28 m, the clear height is 8.12 m, and the clear span of a double tunnel is 32.15 m. The left and right boundaries are taken to the horizontal distance 3D from the tunnel center (D is the diameter of single center circular tunnel), the lower boundary is taken to the vertical distance 3D from the tunnel center, and the upper boundary is taken to the tunnel top ground (tunnel buried depth is 12.9 m). The left and right boundaries are set as horizontal constraints, the bottom as a vertical constraint, and the top as a free surface.

2D-σ establishes the mechanical model, automatically divides the finite element mesh, and optimizes the mesh. The elastic-plastic model, D-P criterion, and plane strain element are used for numerical simulation. The primary support and secondary lining are simulated by the solid element; the bolt is simulated by the rod element.

In the calculation process, the self-weight of the surrounding rock and supporting materials will be loaded automatically, and the lateral pressure coefficient will be calculated according to equation (2). In the calculation process, the role of the shotcrete layer and anchor bolt is reflected by bearing the release load of the in situ stress, i.e., after the tunnel excavation, a part of the original in situ stress is released. The remaining in situ stress of the excavation section is released after the shotcrete layer and

Table 5: Fitting function table of each excavation scheme.

	Excavation scheme I	Excavation scheme II	Excavation scheme III
Point 1	$y = 0.0642\,(x^{29.436}/(444.798^{29.436} + x^{29.436}))$	$y = 0.0916\,(x^{8.049}/(409.059^{8.049} + x^{8.049}))$	$y = 0.0659\,(x^{2.764}/(429.059^{2.764} + x^{2.764}))$
Point 2	$y = 0.2255\,(x^{7.879}/(869.360^{7.879} + x^{7.879}))$	$y = 0.2567\,(x^{6.069}/(781.949^{6.069} + x^{6.069}))$	$y = 0.2854\,(x^{16.605}/(610.395^{16.605} + x^{16.605}))$
Point 3	$y = 0.0532\,(x^{2.521}/(51.170^{2.521} + x^{2.521}))$	$y = 0.0835\,(x^{3.639}/(70.825^{3.639} + x^{3.639}))$	$y = 0.0598\,(x^{3.016}/(70.067^{3.016} + x^{3.016}))$
Point 4	$y = 0.2302\,(x^{12.137}/(842.718^{12.137} + x^{12.137}))$	$y = 0.2401\,(x^{7.733}/(736.734^{7.733} + x^{7.733}))$	$y = 0.2792\,(x^{19.602}/(442.783^{19.602} + x^{19.602}))$
Point 5	$y = 0.0679\,(x^{7.128}/(440.462^{7.128} + x^{7.128}))$	$y = 0.0827\,(x^{12.187}/(410.937^{12.187} + x^{12.187}))$	$y = 0.0593\,(x^{1.450}/(329.319^{1.450} + x^{1.450}))$

Table 6: Statistics of maximum displacement.

	Maximum displacement of model (mm)	Actual maximum displacement (mm)
Excavation scheme I	0.23	10.35
Excavation scheme II	0.27	12.15
Excavation scheme III	0.29	13.05

anchor bolt are installed. The release rate of in situ stress shall be determined in combination with the actual measurement results of tunnel engineering and the construction experience of engineers. In this finite element calculation, the in situ stress release rate of each stage is 20% of the surrounding rock, 20% of the initial support, and 60% of the secondary lining. Assuming that the tunnel construction is uniformly advanced, the rheological effect of the surrounding rock near the excavation surface is not considered, however, the spatial effect alone of the excavation surface is considered.

$$\lambda = \frac{\mu}{1-\mu}, \tag{2}$$

where λ is the lateral pressure coefficient and μ is Poisson's ratio of the surrounding rock.

4.3. Result Analysis

4.3.1. Maximum Principal Stress. Firstly, the maximum principal stress of scheme I is analyzed (Figure 7):

Left wall: the maximum principal stress of this part does not change significantly during the construction of the middle wall, however, when the left pilot tunnel is constructed, the stress of the surrounding rock is released, and the stress relaxation coefficient is about 69%. During the construction of the right tunnel, the impact on the maximum principal stress at this point is also very small, but the maximum principal stress of surrounding rock will increase during the construction of left main tunnel. However, it has not reached the original stress and only recovered to 72% of the original stress.

Left vault: the maximum principal stress does not change significantly during the construction of the middle wall and pilot tunnels on both sides, and its value only decreases by 2.3%. However, during the construction of the right tunnel, the stress at this place increases. Compared with the original state, the maximum principal stress increases by 3.6%. During the construction of the main tunnel of the left tunnel, the stress at this place decreases sharply, and the final maximum principal stress is only 33.5% of the original stress. The stress relaxation coefficient is 66.5%.

Middle wall top: the maximum principal stress will decrease during the construction of the middle pilot tunnel, but with the progress of construction, especially the construction of the main tunnels on both sides, the surrounding rock pressure will increase, and finally, the maximum principal stress of the surrounding rock will reach 230.5% of the original state.

Right vault: the maximum principal stress does not change significantly during the construction of the middle wall and side pilot tunnels on both sides, and its value only decreases by 3.0%. However, during the construction of the right tunnel, the stress at this place will decrease sharply. Finally, the maximum principal stress is only 26.2% of the original stress, and the stress relaxation coefficient is 73.6%. During the construction of the left tunnel, the stress at this place will increase, and the maximum principal stress increases to 36.1% of the original stress.

Right wall: the maximum principal stress at this part will gradually decrease during the construction of the upper steps of the middle pilot tunnel and right main tunnel, and the minimum value is only 29.2% of the initial stress. However, with the construction of the secondary lining of the right tunnel and the construction steps, the maximum principal stress increases, and finally, it reaches 60.6% of the original state.

Secondly, the maximum principal stress of scheme II is analyzed (Figure 8):

Left wall: this index has little change during the construction of the middle wall, but when the left pilot tunnel is constructed, the stress of the surrounding rock is released, and the stress relaxation coefficient is 71.7%. During the construction of the right tunnel, the impact on the maximum principal stress at this point is also very small, but during the construction of the main tunnel of the left tunnel, the maximum principal stress of the surrounding rock will increase, but it has not returned to the original stress, which is 73.6% of the original stress.

Left vault: during the construction of the middle wall and side pilot tunnels on both sides, the change is not obvious. Its value only decreases by 1.6%. However, during the construction of the right tunnel, the stress will increase, which increases by 6.0% compared with the original state. During the construction of the main tunnel of the left tunnel, the stress will decrease sharply. Finally, the value is only 27.1% of the original stress, and the stress relaxation coefficient is 72.9%.

Middle wall top: it will decrease during the construction of the middle pilot tunnel. However, with the progress of construction, especially the construction of the main tunnels on both sides, the surrounding rock pressure will increase, and finally, the maximum principal stress of the surrounding rock will reach 226.7% of the original state.

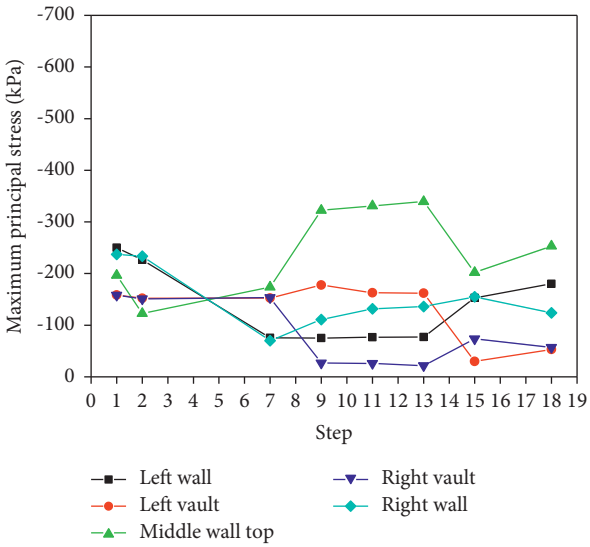

Figure 7: Maximum principal stress of scheme I.

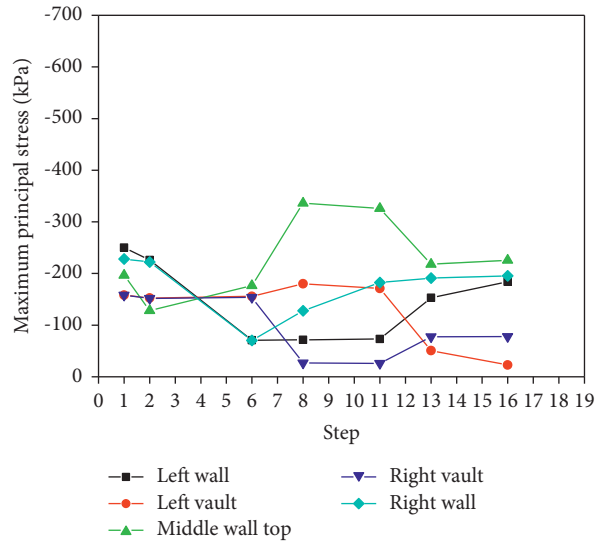

Figure 8: Maximum principal stress of scheme II.

Right vault: during the construction of the middle wall and side pilot tunnels on both sides, the change of this part is not obvious, and its value only decreases by 2.7%. However, during the construction of the right tunnel, the stress will decrease sharply. Finally, the value is only 29.0% of the original stress, and the stress relaxation coefficient is 71.0%. During the construction of the main tunnel of the left tunnel, the stress will increase, and finally, it will reach 29.2% of the original stress.

Right wall: this part will gradually decrease during the construction of the upper steps of the middle pilot tunnel and the right main tunnel. The minimum value is only 28.2% of the initial stress. However, with the construction of the secondary lining of the right tunnel and the construction steps, the maximum principal stress increases, and finally, it reaches 78.6% of the original state.

Finally, the maximum principal stress of scheme III is analyzed (Figure 9):

Left wall: this index changes little during the construction of the middle wall and right tunnel. However, during the construction of the left tunnel, the stress of the surrounding rock is released. The stress relaxation coefficient is 78.1%, and the stress value is 21.9% of the original stress.

Left vault: during the construction of the middle wall and the left tunnel, the index changes very little. After the construction of the right tunnel, the index only decreases by 5.2%. During the construction of the upper step of the right tunnel, a lot of stress is released, and the index decreases greatly, which is only 32.0% of the original in situ stress. The construction of the lower step of the left tunnel has little impact on the stress at this place, which only increases by 2.2% when compared with the upper step.

Middle wall top: during the construction of the middle pilot tunnel, the stress is released, and this value decreases to 72.8% of the original in situ stress. With the construction of the main tunnels on the left and right sides, this value gradually increases, and finally, it increases to 236.0% of the original in situ stress.

Right vault: during the construction of the middle pilot tunnel and the upper step of the right tunnel, the stress value at this position gradually decreases, and the minimum value is only 36.2% of the original stress state. With the construction of the lower step of the right tunnel and the left tunnel, the stress value at this position gradually increases, and finally, it returns to 51.8% of the original in situ stress.

Right wall: this part increases sharply during the construction of the middle pilot tunnel and right upper step. After the construction of the upper step of the right tunnel, the stress increases to 263.8% of the original in situ stress. During the construction of the lower step, the stress decreases sharply, and the stress value decreases to 235.1% of the original in situ stress. The construction of the left tunnel has little impact on the stress. When the secondary lining of the left tunnel is completed, this value is still 222.2% of the original in situ stress.

4.3.2. Minimum Principal Stress. Firstly, the minimum principal stress of scheme I is analyzed (Figure 10):

Left wall: the minimum principal stress increases continuously with the progress of construction. During the construction of the middle pilot tunnel, its value increases by 3.5% alone. However, during the construction of the left pilot tunnel, the stress increases by 28.7%. During the construction of the left tunnel, the minimum principal stress does not change significantly. During the construction of the left tunnel, the

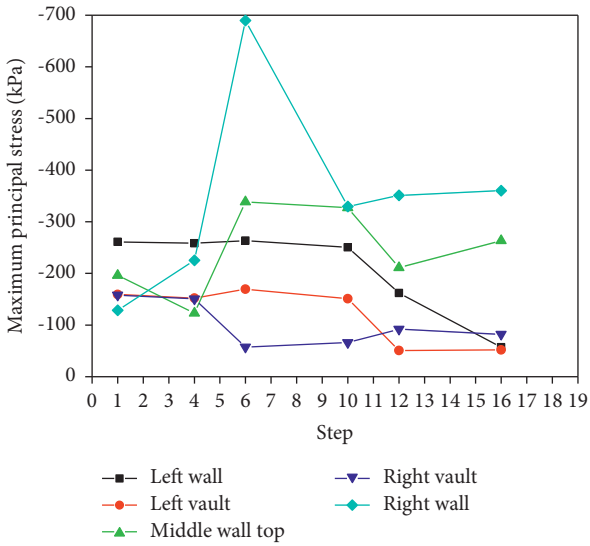

Figure 9: Maximum principal stress of scheme III.

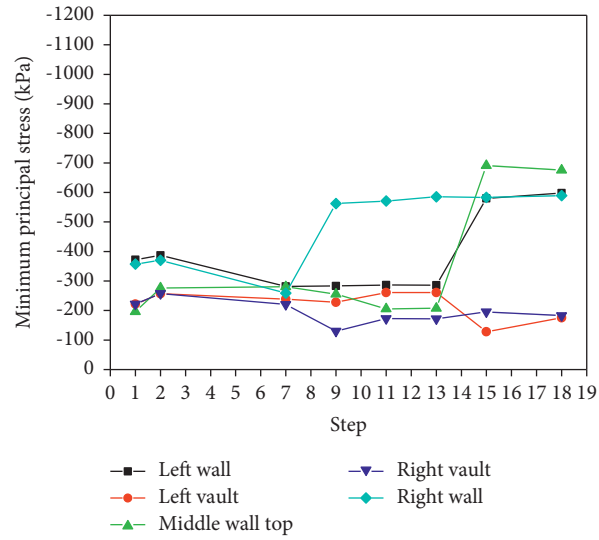

Figure 10: Minimum principal stress of scheme I.

minimum principal stress increases significantly when compared with the original stress, which is an increase of 59.8%.

Left vault: the minimum principal stress will increase slightly during the construction of the pilot tunnel and right main tunnel. However, the stress will also decrease during the construction of the left tunnel. Finally, the minimum principal stress is only 72.2% of the original stress.

Middle wall top: the minimum principal stress increases with the progress of construction, and finally, it reaches 322.7% of the initial stress.

Right vault: the minimum principal stress will increase slightly during the construction of the pilot tunnel. However, the stress will also decrease sharply during the construction of the right tunnel, which is 71.1% of the initial stress. With the construction of the left tunnel, the final minimum principal stress will return to 75.6% of the original stress.

Right wall: the minimum principal stress increases with the progress of construction from 357.3 kPa of the original stress to 289.1 kPa, with an increase of 162.9%.

Secondly, the minimum principal stress of scheme II is analyzed (Figure 11):

Left wall: with the progress of construction, the value of the middle pilot tunnel increased by only 3.1%. However, during the construction of the left pilot tunnel, the stress increased by 29.0%. During the construction of the left main tunnel, the minimum principal stress did not change significantly. During the construction of the left main tunnel, the minimum principal stress increased significantly, an increase of 81.5% relative to the original stress.

Left vault: it will rise slightly during the construction of the pilot tunnel and right main tunnel. However, the stress will also decrease during the construction of the left tunnel. Finally, the value is only 71.8% of the original stress.

Middle wall top: it increases with the progress of construction, and finally, it reaches 233.9% of the initial stress.

Right vault: it will rise slightly during the construction of the pilot tunnel. However, the stress will also decrease sharply during the construction of the right tunnel, which is 71.6% of the initial stress. With the construction of the left tunnel, this value will return to 83.2% of the original stress.

Right wall: with the progress of construction, the original stress increased from 373.0 kPa to 682.2 kPa, with an increase of 183.9%.

Finally, the minimum principal stress of scheme III is analyzed (Figure 12):

Left wall: with the progress of construction, the value of the middle pilot tunnel and the right tunnel changed little during the construction. It only increased by 3.7%, but the stress increased significantly during the construction of the upper and lower steps of the left tunnel, an increase of 166% relative to the original stress.

Left vault: during the construction of the middle pilot tunnel and right tunnel, the change of this index is relatively small, with an increase of only 12.0%. However, during the construction of the upper steps of the left tunnel, this index declines sharply, and this value is only 56.9% of the original condition. During the construction of the lower steps of the left tunnel, this value has increased slightly, reaching 67.0% of the original stress.

Middle wall top: this value also decreases during the construction of the middle pilot tunnel. With the construction of the main tunnels on the left and right sides, the stress value gradually increases, and the maximum value increases to 238.7% of the original in situ stress.

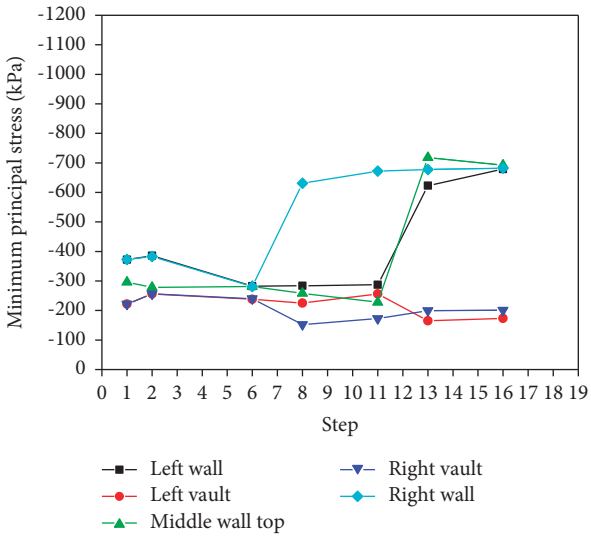

Figure 11: Minimum principal stress of scheme II.

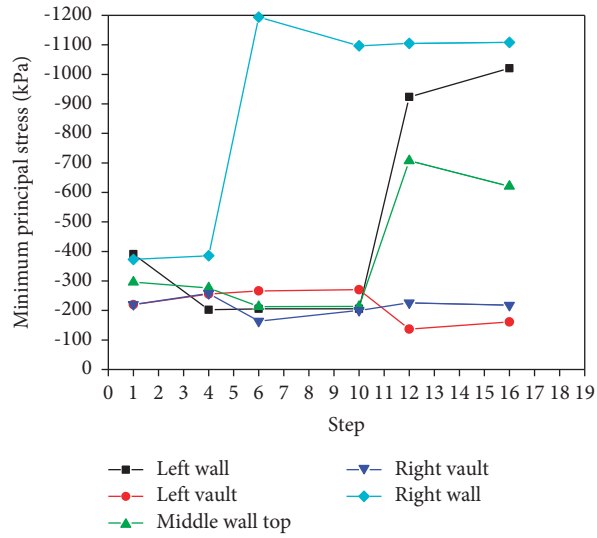

Figure 12: Minimum principal stress of scheme III.

Right vault: during the construction of the pilot tunnel, the stress will rise slightly. However, during the construction of the upper step of the right tunnel, the stress will decrease sharply, which is 68.1% of the initial stress. With the construction of the lower step and left tunnel, the value will return to 90.6% of the original stress.

Right wall: during the construction of the middle pilot tunnel, the stress value changes little. However, with the construction of the upper step of the right tunnel, the index increases sharply, reaching 320.0% of the original in situ stress. During the construction of the lower step, the index will decrease by 8.1%. The construction of the left tunnel basically has no impact on the index.

4.3.3. Displacement. Firstly, the displacement of scheme I is analyzed (Figure 13):

Left wall: the displacement at this place is small. During the construction of the side pilot tunnel, the displacement reaches the maximum, which is 0.9 mm. With the progress of construction, the displacement at this place decreases, and the final displacement is only 0.5 mm.

Left vault: the displacement at this location is large. During the construction of pilot tunnel, the displacement at this location is only 0.6 mm. During the construction of the right tunnel, the displacement at this location nearly doubled to 1.2 mm. During the construction of the main tunnel of the left tunnel, the displacement at this location increased rapidly to 3.1 mm.

Middle wall top: the displacement at this place is small, and the maximum value is only 2.0 mm. During the construction of the upper steps of the right main tunnel, the settlement at this place reaches the maximum value of 2.0 mm. After the construction of the secondary lining, the settlement of the surrounding rock at this place shows an upward trend, and the final displacement returns to 1.3 mm.

Right vault: the displacement at this place is relatively large. During the construction of the pilot tunnel, the displacement at this place is only 0.6 mm. During the construction of the right tunnel, the displacement at this place increases rapidly, reaching 3.2 mm. With the construction of the secondary lining and main tunnel of the left tunnel, the settlement at this place rises somewhat, and finally, it stabilizes at 2.8 mm.

Right wall: the displacement at this place is small. During the construction of the side pilot tunnel, the displacement reaches the maximum, which is 0.9 mm. With the progress of construction, the displacement at this place decreases, and the final displacement is only 0.5 mm.

Secondly, the displacement of scheme II is analyzed (Figure 14):

Left wall: the displacement at this place is small. During the construction of the side pilot tunnel, the displacement reaches the maximum, which is 0.9 mm. With the progress of construction, the displacement at this place decreases, and the final displacement is only 0.8 mm.

Left vault: the displacement at this place is large. During the construction of the pilot tunnel, the displacement at this place is only 0.6 mm. During the construction of the right tunnel, the displacement at this place basically does not change. During the construction of the main tunnel of the left tunnel, the displacement at this place increases rapidly, reaching 3.9 mm.

Middle wall top: the displacement at this place is small, and the maximum value is only 1.3 mm. During the construction of the right lower step, the settlement at this place reaches the maximum value of 1.3 mm. After the construction of the secondary lining, the settlement

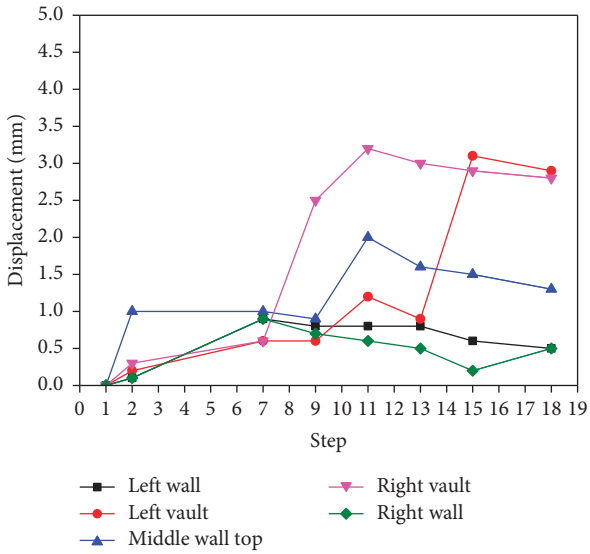

Figure 13: Displacement of scheme I.

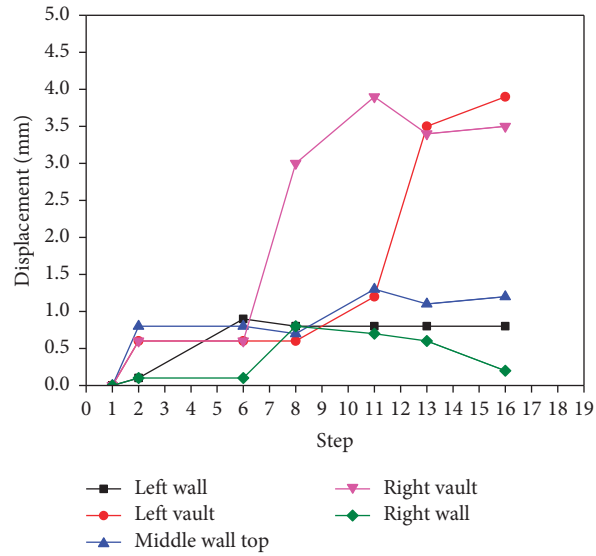

Figure 14: Displacement of scheme II.

of the surrounding rock at this place rebounds slightly, and the final displacement returns to 1.2 mm.

Right vault: the displacement at this location is relatively large. During the construction of the pilot tunnel, the displacement at this location is only 0.6 mm. During the construction of the right tunnel, the displacement at this location increases rapidly, reaching 3.9 mm. With the construction of the main tunnel of the left tunnel, the settlement at this location rebounds, and finally, it stabilizes at 3.5 mm.

Right wall: the displacement at this place is small. During the construction of the side pilot tunnel, the displacement reaches the maximum, which is 0.8 mm. With the progress of construction, the displacement at this place decreases, and the final displacement is only 0.2 mm.

Finally, the displacement of scheme III is analyzed (Figure 15):

Left wall: the displacement at this place is small. During the construction of the upper steps of the right tunnel and left tunnel, the displacement is very small, which is only 0.3 mm. With the construction of the lower steps of the left tunnel, the maximum displacement is 0.8 mm.

Left vault: during the construction of the middle pilot tunnel, the displacement of the surrounding rock is 0.4 mm. During the construction of the right tunnel, the displacement value has not changed. During the construction of the upper step of the left tunnel, the value changes the most, and the settlement reaches 3.1 mm. With the construction of the lower step, the displacement value further increases, and finally, it reaches 4.2 mm.

Middle wall top: during the construction of the middle pilot tunnel, the displacement value at this place reaches the maximum, which is 1.0 mm. With the progress of construction, the displacement is in a fluctuating state, and finally, it stabilizes at 0.9 mm.

Right vault: the displacement at this place is large. During the construction of the pilot tunnel, the displacement at this place is only 0.6 mm. During the construction of the upper steps of the right tunnel, the displacement at this place increases rapidly, reaching 3.5 mm. During the construction of the lower steps, the value will decrease to 3.2 mm. With the construction of the left tunnel, the displacement value reaches the final value of 3.8 mm.

Right wall: the displacement at this place is small. During the construction of the lower step of the right tunnel, the displacement reaches a maximum of 0.3 mm. The construction of the left tunnel basically has no impact on the displacement at this place.

4.3.4. Failure Proximity (Reciprocal of Safety Factor). Firstly, the failure proximity of scheme I is analyzed (Figure 16):

Left wall: during the construction of a side pilot tunnel, the stress of the surrounding rock at this place is the most unfavorable, and the damage proximity reaches 0.82. However, the construction of the main tunnel of the left tunnel is beneficial to stabilize the surrounding rock at this place, and the damage proximity is reduced to 0.67.

Left vault: the surrounding rock here is relatively safe, and the maximum damage proximity is only 0.21.

Middle wall top: the surrounding rock here is relatively safe, and the maximum damage proximity is only 0.35.

Right vault: the surrounding rock here is relatively safe, and the maximum damage proximity is only 0.38.

Right wall: during the construction of the side pilot tunnel, the stress of the surrounding rock at this place is

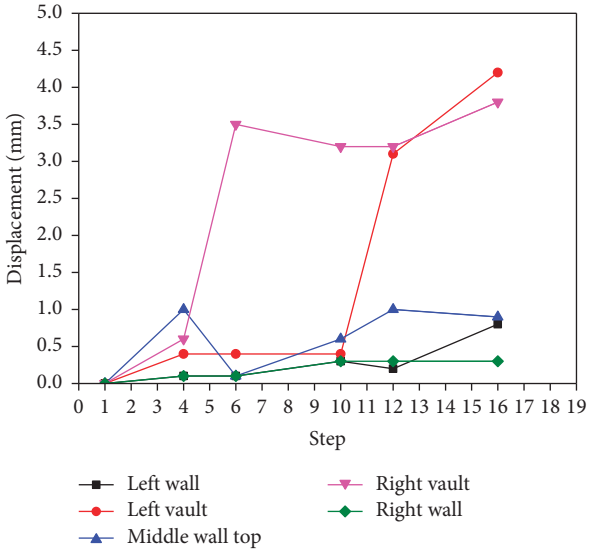

Figure 15: Displacement of scheme III.

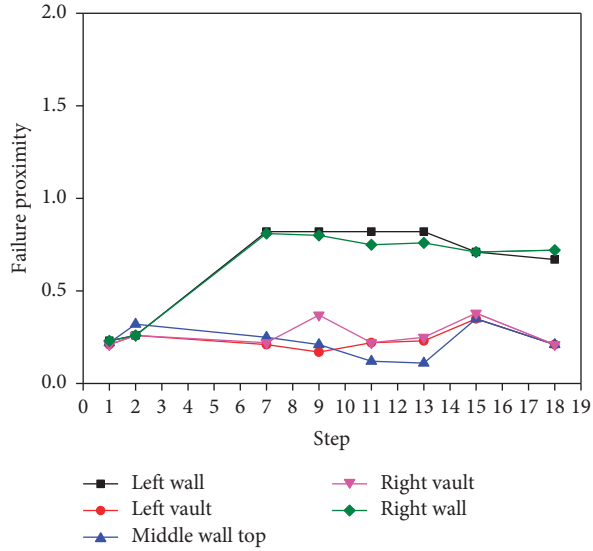

Figure 16: Failure proximity of scheme I.

the most unfavorable, and the damage proximity reaches 0.81. However, the construction of the main tunnel is beneficial to stabilize the surrounding rock at this place, and the damage proximity is finally reduced to 0.72.

Secondly, the failure proximity of scheme II is analyzed (Figure 17):

Left wall: during the construction of the side pilot tunnel, the stress of the surrounding rock at this place is the most unfavorable, and the damage proximity reaches 0.82. However, the construction of the main tunnel of the left tunnel is beneficial to stabilize the surrounding rock at this place, and the damage proximity is reduced to 0.73.

Left vault: the surrounding rock here is relatively safe, and the maximum damage proximity is only 0.25.

Middle wall top: the surrounding rock here is relatively safe, and the maximum damage proximity is only 0.36.

Right vault: the surrounding rock here is relatively safe, and the maximum damage proximity is only 0.22.

Right wall: during the construction of the side pilot tunnel, the stress of the surrounding rock at this place is the most unfavorable, and the damage proximity reaches 0.82. However, the construction of the main tunnel is beneficial to stabilize the surrounding rock at this place, and the damage proximity is finally reduced to 0.71.

Finally, the failure proximity of scheme III is analyzed (Figure 18):

Left wall: during the construction of the middle pilot tunnel and right tunnel, the surrounding rock is in a relatively safe range. However, with the construction of the upper and lower steps of the left tunnel, the surrounding rock tends to be damaged more. During the construction of the upper steps of the right tunnel, the

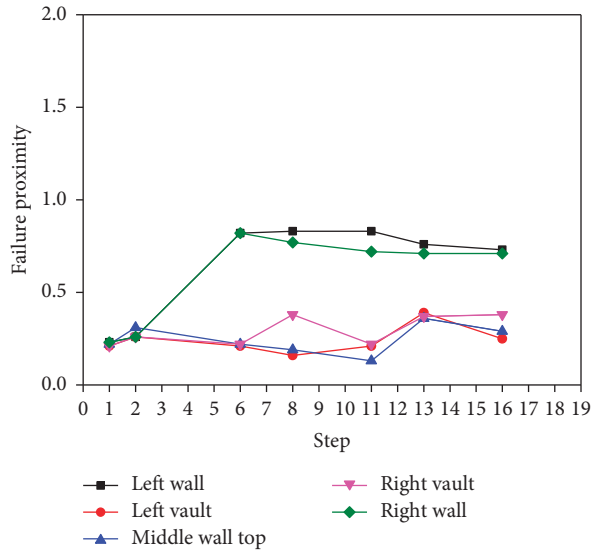

Figure 17: Failure proximity of scheme II.

damage proximity of the surrounding rock reaches 0.93. During the construction of the lower steps of the right tunnel, the damage proximity of the surrounding rock reaches 1.2, and the surrounding rock is in a damaged state.

Left vault: the surrounding rock here is relatively safe, and the maximum damage proximity is only 0.38.

Middle wall top: the surrounding rock here is relatively safe, and the maximum damage proximity is only 0.36.

Right vault: the surrounding rock here is relatively safe, and the maximum damage proximity is only 0.22.

Right wall: the construction of the lower step of the right tunnel is the most unfavorable condition of the surrounding rock, and the damage proximity of the surrounding rock reaches 0.73, while the construction

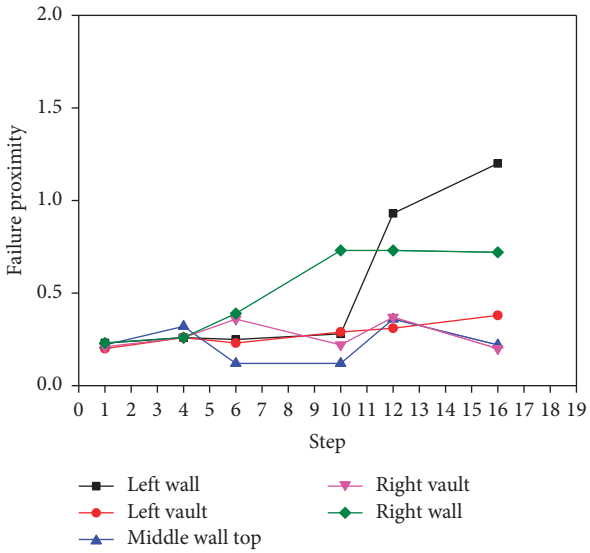

Figure 18: Failure proximity of scheme III.

of the left tunnel basically has no impact on the safety of the surrounding rock.

5. Discussion

The maximum principal stress and minimum principal stress of the sidewall are much greater than those of the vault. This is mainly because of the large excavation span and the flat section. The pressure area generated in the combined structure of the support and surrounding rock increases and is transmitted to the side or arch foot to press against the surrounding rock, especially when the lateral pressure coefficient is small and the vertical stress is the main stress.

Under the condition of class II surrounding rock, when scheme I is adopted for construction, the vault settlement is the smallest, i.e., 3.2 mm. The vault settlement for scheme II is 3.9 mm and that for scheme III is the largest, i.e., 4.2 mm. It can be seen from Figure 19 that no matter which construction scheme is adopted, the displacement of the arch crown is the largest, and the reinforcement of the arch crown is one of the conditions to ensure that the surrounding rock will not be damaged and unstable.

Under the condition of class II surrounding rock, when scheme III is adopted for construction, the damage proximity is the largest, i.e., 1.2, and the left wall is damaged. It can be seen from Figure 20 that no matter which construction scheme is adopted, the damage proximity of the sidewall is the largest, and the reinforcement of the sidewall is one of the conditions to ensure that the surrounding rock will not be damaged and unstable.

Under the condition of class II surrounding rock, when scheme III is adopted for construction, the displacement of the surrounding rock of the arch crown is the largest, and there is a failure zone in the surrounding rock of the sidewall, especially the left wall. In the construction scheme I, although the displacement of the surrounding rock of the arch crown is the smallest, the stress of the lining structure and construction process are complex. Considering the factors,

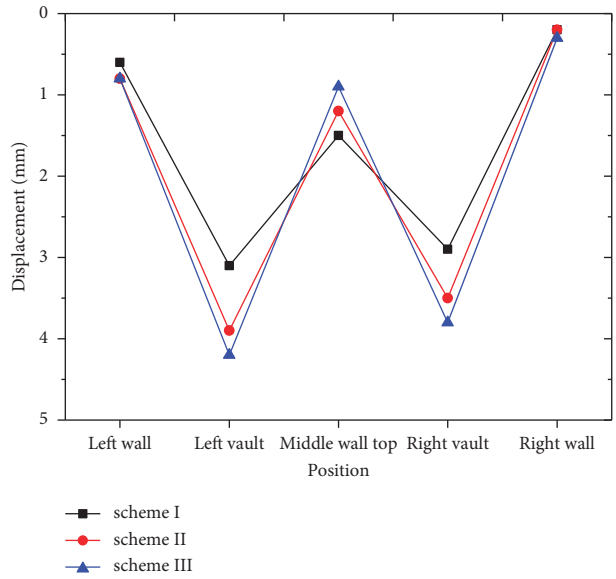

Figure 19: Displacement.

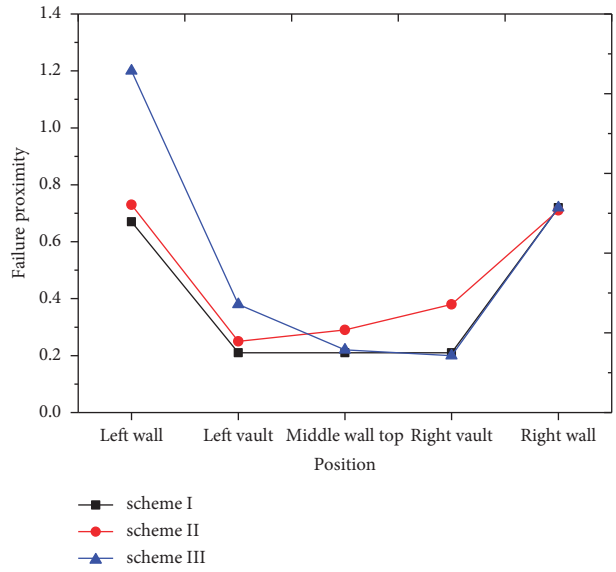

Figure 20: Failure proximity.

such as displacement, stress, damage proximity, and construction process, it is recommended to adopt construction scheme II for construction.

6. Conclusions

Using the simulation test of the six-lane highway multiarch tunnel under different excavation conditions and the analysis of the test data, the following conclusions and suggestions are obtained:

(1) The experimental excavation method is completely consistent with the tunnel construction process, and it solves the problem of simulating the construction state of the highway tunnel

(2) This experiment truly reflects the three-dimensional space problem of excavation and reveals the whole process of the three-stage displacement of the tunnel-surrounding rock

(3) In a weakly weathered sandstone (class II surrounding rock), it is recommended to use the secondary lining integral pouring three heading method (scheme II) for construction

Data Availability

The data used to support the findings of this study are available from the corresponding author upon request.

Conflicts of Interest

The authors declare that they have no known competing financial interests or personal relationships that could have appeared to influence the work reported in this study.

Acknowledgments

This study was supported by the Fundamental Research Funds for Characteristic Innovation Project of Colleges and Universities in Guangdong Province (2020KTSCX288).

References

[1] P. Guo, X. Gong, and Y. Wang, "Displacement and force analyses of braced structure of deep excavation considering unsymmetrical surcharge effect," *Computers and Geotechnics*, vol. 113, 2019.

[2] B. Yuan, Z. Li, Z. Zhao, H. Ni, Z. Su, and Z. Li, "Experimental study of displacement field of layered soils surrounding laterally loaded pile based on transparent soil," *Journal of Soils and Sediments*, vol. 21, no. 9, pp. 3072–3083, 2021.

[3] J. Qiu, Y. Lu, J. Lai, Y. Zhang, and K. Wang, "Experimental study on the effect of water gushing on loess metro tunnel," *Environmental Earth Sciences*, vol. 79, no. 11, 2020.

[4] B. Yuan, Z. Li, Y. Chen et al., "Mechanical and microstructural properties of recycling granite residual soil reinforced with glass fiber and liquid-modified polyvinyl alcohol polymer," *Chemosphere*, vol. 286, p. 131652, 2022.

[5] P. Guo, X. Gong, Y. Wang, H. Lin, and Y. Zhao, "Minimum cover depth estimation for underwater shield tunnels," *Tunnelling and Underground Space Technology*, vol. 115, Article ID 104027, 2021.

[6] S. Hassan and E. Elwakil, "Operational based stochastic cluster regression-based modeling for predicting condition rating of highway tunnels," *Canadian Journal of Civil Engineering*, 2021.

[7] Z. Wang, K. Du, Y. Xie et al., "Buckling analysis of an innovative type of steel-concrete composite support in tunnels," *Journal of Constructional Steel Research*, vol. 179, no. 1, p. 106503, 2021.

[8] X. Chen, Q. Chen, Z. Chen, S. Cai, X. Zhuo, and J. Lv, "Numerical modeling of the interaction between submerged floating tunnel and surface waves," *Ocean Engineering*, vol. 220, p. 108494, 2021.

[9] I. Trabucchi, G. Tiberti, and G. A. Plizzari, "A parametric numerical study on the behavior of large precast tunnel segments during TBM thrust phase," *Engineering Structures*, vol. 241, no. 1, p. 112253, 2021.

[10] S. Li, C. Yuan, X. Feng, and S. Li, "Mechanical behaviour of a large-span double-arch tunnel," *Ksce Journal of Civil Engineering*, vol. 20, no. 7, pp. 1–9, 2016.

[11] Y. Zhao and Z.-g. Zhang, "Mechanical response features and failure process of soft surrounding rock around deeply buried three-centered arch tunnel," *Journal of Central South University*, vol. 22, no. 10, pp. 4064–4073, 2015.

[12] D. J. Curtis, "Visco-elastic tunnel analysis," *Tunnels & Tunnelling International*, vol. 6, 1974.

[13] D. M. Potts and J. H. Atkinson, "Stability of a shallow circular tunnel in cohesionless soil," *Géotechnique*, vol. 27, no. 2, pp. 203–215, 1977.

[14] L. Dormieux, "Upper and lower bound solutions for the face stability of shallow circular tunnels in frictional material," *Géotechnique*, vol. 40, no. 4, pp. 581–606, 1990.

[15] X.-l. Yang and S. Zhang, "Risk assessment model of tunnel water inrush based on improved attribute mathematical theory," *Journal of Central South University*, vol. 25, no. 2, pp. 379–391, 2018.

[16] Z. Zhang, C. Zhang, K. Jiang et al., "Analytical prediction for tunnel-soil-pile interaction mechanics based on kerr foundation model," *KSCE Journal of Civil Engineering*, vol. 23, no. 6, pp. 2756–2771, 2019.

[17] K. Miura, H. Yagi, H. Shiroma, and K. Takekuni, "Study on design and construction method for the New Tomei-Meishin expressway tunnels," *Tunnelling & Underground Space Technology Incorporating Trenchless Technology Research*, vol. 18, no. 2/3, pp. 271–281, 2003.

[18] C. S. Wu, J. X. Li, X. Chen, and Z. P. Xu, "Blasting in twin tunnels with small spacing and its vibration control," *Tunnelling and Underground Space Technology*, vol. 19, no. 19, p. 518, 2004.

[19] Z. Liu, M. He, and H. Xiao, "Deformation monitoring and control measures of shallow large-span duel-linked arch tunnel," *Chinese Journal of Geotechnical Engineering*, vol. 25, no. 3, pp. 339–342, 2003, in chinese.

[20] G. Yang, Y. Ge, W. Peng, and W. Liu, "In-situ testing analysis of compound curved middle wall of multi-arch tunnel," *J. Huazhong Univ. of Sci.&Tech. (Natural Science Edition)*, vol. 47, no. 01, pp. 60–64, 2019, in chinese.

[21] B. Yuan, Z. Li, Z. Su, Q. Luo, M. Chen, and Z. Zhao, "Sensitivity of multistage fill slope based on finite element model," *Advances in Civil Engineering*, vol. 2021, pp. 1–13, Article ID 6622936, 2021.

[22] X. Zhang, J. Su, and Y. Xu, "Experimental and numerical investigation the effects of insufficient concrete thickness on the damage behaviour of multi-arch tunnels," *Structure*, vol. 33, 2021.

[23] H. Yoshimura, T. Yuki, Y. Yamada, and N. Kokobun, "Analysis and monitoring of the Miyana railway tunnel constructed using the New Austrian Tunnelling Method," *International Journal of Rock Mechanics and Mining Science & Geomechanics Abstracts*, vol. 23, no. 4, p. 159, 1986.

[24] N. Barton, "Some new Q-value correlations to assist in site characterisation and tunnel design," *International Journal of Rock Mechanics and Mining Sciences*, vol. 39, no. 2, pp. 185–216, 2002.

[25] K. M. Lee and R. K. Rowe, "Finite element modelling of the three-dimensional ground deformations due to tunnelling in soft cohesive soils: Part I - method of analysis," *Computers and Geotechnics*, vol. 10, no. 2, pp. 87–109, 1990.

[26] S.-c. Li, H.-l. Liu, L.-p. Li, Q.-q. Zhang, K. Wang, and K. Wang, "Large scale three-dimensional seepage analysis

model test and numerical simulation research on undersea tunnel," *Applied Ocean Research*, vol. 59, pp. 510–520, 2016.

[27] C. Liu, H. Yang, X. Jiang, and H. Shi, "Shaking table test and numerical simulation for acceleration response laws of shallow-buried biased double-arch tunnel," *Journal of Vibroengineering*, vol. 21, no. 4, pp. 1188–1200, 2019.

[28] B. Min, C. Zhang, X. Zhang, H. Wang, P. Li, and D. Zhang, "Cracking performance of asymmetric double-arch tunnels due to the voids behind linings," *Thin-Walled Structures*, vol. 154, p. 106856, 2020.